Strength coupling in mixed phases under high pressure

Xiaozhi Yan, Haini Dong, Guangai Sun, Xiangting Ren, Duanwei He, and Wenge Yang

Phys. Rev. B **94**, 144104 — Published 21 October 2016

DOI: 10.1103/PhysRevB.94.144104

Strength Coupling in Mixed Phases under High Pressure

Xiaozhi Yan,[1,2,*] Haini Dong,[2,3] Duanwei He[4,*] and Wenge Yang[2,5,*]

[1]*Institute of Nuclear Physics and Chemistry, China Academy of Engineering Physics, Mianyang 621900, China;*

[2]*Center for High Pressure Science and Technology Advanced Research (HPSTAR), Shanghai 201203, P. R. China;*

[3]*Key Laboratory of High-temperature and High-pressure Study of the Earths Interior, Institute of Geochemistry, Chinese Academy of Sciences, Guiyang, Guizhou 550081, China;*

[4]*Institute of Atomic and Molecular Physics, Sichuan University, Chengdu 610065, P. R. China;*

[5]*High Pressure Synergetic Consortium (HPSynC), Geophysical Laboratory, Carnegie Institution of Washington, Argonne, Illinois 60439, USA.*

[*]To whom correspondence should be addressed. E-mail: yxzdsb000000@163.com; duanweihe@scu.edu.cn; yangwg@hptar.ac.cn

The strength of a material can be altered by temperature, pressure, grain size and orientation distributions. At the microscale neighboring grains often play important roles in the elastic and plastic deformation process. By applying high pressure to a mixture of germanium and gold powder in the vicinity of the germanium phase transition pressure, we found the deformation behavior of gold largely correlates with that of the surrounding germanium. The deviatoric strain and compressibility of Au behaves anomalously when Ge undergoes a diamond to β-tin structure transition,

accompanying a large volume and strength drop. The results demonstrate that the intrinsic strength of a mixed phase could be largely controlled by the other surrounding phase, which is fundamentally important in understanding the deformation mechanism of multi-phase materials, especially when one phase undergoes dramatic changes in strength under high pressure conditions.

I. INTRODUCTION

In a single crystal, the plastic deformation is mainly controlled by the motion of defects. Therefore, the plastic behavior of single crystallized materials depends on temperature and pressure which have influence on the defect motion activation [1-3]. In single-phase polycrystalline materials, defects may be stopped and pile up at grain boundaries and/or triple junctions, which often enhance the strength of the materials [4, 5]. As the applied stress required for moving a dislocation across a grain increases with decreasing grain size, the strength of a polycrystalline material with smaller grain size is expected to be higher. This increase in strength is known as the Hall-Petch effect which has been frequently used to design materials with exceptional properties [4-7].

The micro-mechanism of deformation in a multiphase material is more complicated. Experimental observations suggest that the plastic deformation of a multi-phase material is controlled not only by the strength of each phase but also the stress/strain distribution across both grain boundaries of the same and different phases [8, 9]. To simplify this puzzle, the invariable strength of each phase was implemented

to quantify the bulk strength of multi-phase composites [8, 10, 11], while there is not a good match between experimental results and theoretical predictions [10, 11].

In fully compacted materials, a grain cannot deform plastically until it meets the requirement of the compatibility of strain from its neighboring grains because their continuity must be maintained during the deformation [8]. In other words, the deformation of a grain is constrained by the materials around it. If the surrounding grains of one crystal were replaced by a softer phase, the constraint on this crystal might be released by activating defects more easily, which reduces the strength and restraints the texture development. To improve the existing models, we applied in-situ high pressure to the mixed phase of gold (Au) and germanium (Ge) powder. In the vicinity of Ge phase transition pressure, the strength of Ge has a large drop during the semiconducting diamond structure (Ge-I) to a metallic β-tin structure (Ge-II) transition [12, 13]. Our previous results show that Ge softens first and hardens later during this phase transition [13], which provides an ideal candidate for this task. Under such a highly confined pressure (10 GPa and above), the mixed powders of Au and Ge is compressed tightly with intimate grain boundaries between the same or different phases. Synchrotron x-ray diffraction (XRD) in radial and axial modes were applied to measure the elastic and plastic deformation for both the Ge and Au phases. We found that the strain evolution of Au follows well with the deformation process of Ge, which suggests a strong strength coupling between these two materials.

II. EXPERIMENT

High-pressure axial x-ray diffraction (AXRD) and radial x-ray diffraction (RXRD) were carried out at the 16BM-D station of the High-Pressure Collaborative Access Team (HPCAT), at the Advanced Photon Source, Argonne National Laboratory. The monochromatic x-ray beam was focused to 10 (vertical) × 7 (horizontal) μm^2 in full width at half maximum (FWHM). The powder of Ge and Au with a 4:1 volumetric ratio was mixed thoroughly as a pristine sample. The starting crystalline size is about 1 μm for Ge and 0.5 μm for Au. For the AXRD measurements, the mixture of Ge and Au powder was loaded into a 100-μm-diameter hole drilled in a stainless steel gasket with a symmetrical diamond anvil cell (DAC), while the mixture was loaded in a 60-μm-diameter hole drilled in a boron-epoxy gasket with a panoramic DAC for the RXRD measurement. For both cases, a pair of 300 μm culet anvils was used. The pressures were obtained from the first four diffraction peaks of Au in the two experiments with its known equation of state [14]. No pressure media were used in these experiments to produce enough differential stress to deform the sample. The XRD data were collected with a Mar345 area detector in the angle-dispersive mode, and processed with the Fit2d [15] and MAUD Rietveld refinement programs [16].

III. RESULTS AND DISCUSSION

Upon compression, the onsite phase transition of Ge I to Ge II started around 9.5 GPa, consistent with previous experimental reports [12, 17]. Further compression increases in the volumetric ratio of the amount of Ge-II to that of Ge-I (Figure 1a). At

13.8 GPa, the phase transformation is complete. The AXRD pattern and its Rietveld refinement at 11.7 GPa are shown in Figure 1b, where both Ge-I and Ge-II phases, as well as Au, are present. Heterogeneous deviatoric strain in each crystal grain of the powder sample, together with the small grain size effect, gives rise to XRD peak broadening. In the case of AXRD, the Scherrer equation is usually used to de-convolute grain size and the strain effect on the diffraction line widths [18]:

$$FWHM^2\cos^2\theta = (\frac{\lambda}{d})^2 + \sigma^2\sin^2\theta \qquad (1)$$

where *FWHM* is the full-width at half-maximum of the diffraction peak on 2θ-scale. The symbols d, λ, and σ denote the grain size, X-ray wavelength, and deviatoric strain, respectively.

The deviatoric strain vs pressure for Ge-I, Ge-II and Au are plotted in Figure 2. The deviatoric strain of both Ge-I and Au increase with pressure until the phase transition of Ge starts. Owing to the large volumetric mismatch strain (about 19% volume decrease from Ge-I to Ge-II) during the transition [12], the deviatoric strain of both Ge-I (Figure 2a) and Ge-II (Figure 2b) released at the early stages of transformation and followed by an increase with pressure. Interestingly, the deviatoric strain of Au also decreases first while increases later (Figure 2c), following the evolution of Ge. This is quite different from earlier non-hydrostatic compression results of Au powder with both axial and radial diffraction geometries, in which the differential strain of Au increases nearly linearly with pressure up to about 60 GPa [19, 20]. After the phase transition of Ge , the deviatoric strain of Au showed no obvious variation, just like that of Ge-II. All of these features indicate a strong strength

coupling of Ge and Au grains.

The plastic deformation of Au could also be manifested by the unusual compressibility of different lattices. When plastic deformation starts, the dislocation slip systems operate within the grain sets, followed by the grain rotation and texture development [21-23]. As a result, stress redistributes in the grains and the measured compressibility of different lattices will show discontinuity [24, 25]. In AXRD experiments, the normal directions of the detected lattice planes are within 11 degrees (2 theta within 22 degrees as shown in Figure. 2) from the loading force direction (Figure 3a). Figure 3b shows the ratios of the *d*-spacings of different lattice planes for Au in AXRD experiments. The d_{hkl}/d_{220} (d_{hkl} represents the d-spacing of (*h k l*) lattice plane) ratio of Au changes slightly with pressure before the phase transition of Ge, then increases sharply with pressure in the early phase transition of Ge and decreases in the latter stage of transformation.

Texture of Au at the middle of the Ge phase transition pressure (11.9 GPa) is shown in Figure. 3c in the form of an inverse pole figure (IPF). The maximum IPF of the compression direction is at the (110) corner, indicating that the readily developed (110) texture is formed, consistent with {111}<110> slip of *fcc* crystals [25, 26]. This demonstrates that the {220} grain family of Au rotated toward the direction parallel to the loading direction. For the Au grains with (220) planes nearly perpendicular to the loading direction, the shear stress in gold grains under less lateral stress is larger and easier to deform under a certain vertical loading force. Consequently, the grains bearing smaller lateral stress are apt to yield and rotate first, while the others under

larger lateral stress stay there (which is indicated by the minimum IPFs of the rolling direction and transverse direction at (110) corner (Figure 3c)), and the resulting d_{220} measured in AXRD experiments exhibits a compressive shift. Thereby, the ratios of the *d*-spacings of other lattice planes to the (220) plane increase during deformation as seen in Figure 3b. In the latter stage of the phase transition of Ge, the plastic deformation in Au particles ceases due to the hardening of Ge, and under further compression the Au particles have a chance to stay under relative low lateral stress. As a result, the load distribution of the grains restores to the previous level and the ratio of the *d*-spacing of other lattice planes to (220) plane decreases to the normal value (Figure 3b).

These findings may have implications for understanding the plastic deformation effect on elastic anisotropy in mixed phases under high pressure. The elastic anisotropy represents the difference of elastic modulus at different crystallographic directions and should be an important intrinsic property of the materials. The results from this work demonstrated that the abnormal evolution of d_{hkl}/d_{220} ratios during the deformation of Au when the surrounding Ge was under large volume collapse (phase transition), indicating that the measured elastic strain can be controlled by the plastic anisotropy once plastic flow is initiated and the elastic strain anisotropy may be modified by the plastic flow. Thus the plastic flow can invalidate measurements of elastic moduli [27-30]. Furthermore, as mentioned above, the pressure distribution in grains with different orientations depends on the activated slip systems, thus the measured elastic strain anisotropy should be related to the activated slip system in

sample.

Two schemes may be involved to the coupling between the deformation behaviors of Au and Ge grains. First, according to the grain boundary strengthening theory [8], under an applied stress, dislocations in Ge grains may pile up near the boundaries between the Ge and Au grains, generating a repulsive force to the dislocations at the Au grain side. As a consequence, the propagation of dislocations in Au grains is blocked which causes increasing deviatoric strain in Au. Once the large plastic deformation in Ge releases, (i.e., the dislocations accumulated near grain boundary start to slip and exit to the grain surface) the resistance of the dislocation slip in the Au side will also be reduced which leads to the deformation of Au. Additionally, the SEM observations of the sample quenched from 10.65 GPa (Figure 4) indicated that the mixed sample is tightly compacted during the phase transition of Ge, the continuity of the Ge-Au mixture needs to be maintained. Therefore the deformation of Ge needs to be accommodated by the deformation of Au.

IV. CONCLUSIONS

Our in-situ high pressure XRD results show that the deformation of Au is activated by the deformation of Ge in the mixture, and demonstrates that the plastic behavior of one material correlates to the strength of the other materials mixed with it. This finding may shed light on the understanding of the deformation behavior of multiphase solids, particular of the rheological behavior of Earth materials, which are usually comprised of multiphase materials.

ACKNOWLEDGMENTS

This work was financially supported by the China 973 Program (Grant No. 2011CB808200), and the National Natural Science Foundation of China (Grant No. 11027405 and U1530402). W. Y. acknowledges the financial support from DOE-BES X-ray Scattering Core Program under grant number DE-FG02-99ER45775. HPCAT operations are supported by DOE-NNSA under Award No. DE-NA0001974 and DOE-BES under Award No. DE-FG02-99ER45775, with partial instrumentation funding by NSF. APS is supported by DOE-BES, under Contract No. DE-AC02-06CH11357.

REFERENCES

[1] A. E. Gleason and W. L. Mao, Nat. Geosci. **6**, 571 (2013).

[2] J. Chen, D. J. Weidner and M. T. Vaughan, Nature **419**, 824 (2002).

[3] T. S. Duffy, R. J. Hemley and H. K. Mao, Phys. Rev. Lett. **74**, 1371 (1995).

[4] E. O. Hall, Proc. Phys. Soc. B **64**, 747 **(**1951).

[5] N. J. Petch, J. Iron Steel Inst. **174**, 25 (1953).

[6] V. L. Solozhenko, O. O. Kurakevych, and Y. Le Godec, Adv. Mater. **24**, 1540 (2012).

[7] Q. Huang, D. Yu, B. Xu, W. Hu, Y. Ma, Y. Wang, Z. Zhao, Bin Wen, J. He, Z. Liu, and Y. Tian, Nature **510,** 250 (2014).

[8] M S. Paterson, Materials Science for Structural Geology[M]. Springer, 2013.

[9] S. Karato, *Deformation of earth materials: an introduction to the rheology of solid*

earth. (Cambridge University Press, New York, 2008), p. 214.

[10] D. L. Kohlstedt, B. Evans and S. J. Mackwell, J. Geophys. Res. **100**, 17587 (1995).

[11] S. Ji, Z. Wang, and R. Wirth, Tectonophysics, **341**, 69 (2001).

[12] C. S. Menoni, J. Z. Hu, and I. L. Spain, Phys. Rev. B **34**, 362 (1986).

[13] X. Yan, D. Tan, X. Ren, W. Yang, D. He, and H. K. Mao, App. Phys. Lett. **106**, 171902 (2015).

[14] Y. Fei, A. Ricolleau, M. Frank, K. Mibe, G. Shen and V. Prakapenka, Proc. Natl. Acad, Sci. USA **104**, 9182 (2007).

[15] A. P. Hammersley, S. O. Svensson, M. Hanfland, A. N. Fitch and D. Hausermann, High Press Res. **14**, 235 (1996).

[16] L. Lutterotti, S. Matthies, H. Wenk, A. S. Schultz, and J. W. Richardson, J. Appl. Phys. **81**, 594 (1997).

[17] X. J. Chen, C. Zhang, Y. Meng, R. Q. Zhang, H. Q. Lin, V. V. Struzhkin and H. K. Mao, Phys. Rev. Lett. **106**, 135502 (2011).

[18] A. K. Singh, A. Jain, H. P. Liermann, and S. K. Saxena, J. Phys. Chem. Solids **67**, 2197 (2006).

[19] A. K. Singh, H. P. Liermann, S. K. Saxena, H. K. Mao, and S. Usha Devi, J. Phys. Condens. Matter. **18**, S969 (2006).

[20] T. S. Duffy, G. Shen, J. Shu, H. K. Mao, R. J. Hemley and A. K. Singh, J. Appl. Phys. **86**, 6729 (1999).

[21] M. R. Daymond, C. N. Tomé and M. A. M. Bourke, Acta Mater. **48**, 553 (2000).

[22] B. Clausen, T. Lorentzen and T. Leffers, Acta Mater. **46**, 3087 (1998).

[23] J. W. L. Pang, T. M. Holden and T. E. Mason, Acta Mater. **46**, 1503 (1998).

[24] B. Clausen, T. Lorentzen, M.A.M. Bourke, and M.R. Daymond, Mater. Sci. Eng. A **259**, 17 (1999).

[25] H. Li, H. Choo, Y. Ren, T. A. Saleh, U. Lienert, P. K. Liaw and F. Ebrahimi, Phys. Rev. Lett. **101**, 015502 (2008).

[26] B. Chen, K. Lutker, J. Lei, J. Yan, S. Yang and H. K. Mao, Proc. Natl. Acad, Sci. USA **111**, 3350 (2014).

[27] D. J. Weidner, L. Li, M. Davis, J. Chen, Geophys. Res. Lett. **31**, L06621 (2004).

[28] D. J. Weidner and L. Li, J. Phys.: Condens. Matter **18**, S1061 (2006).

[29] S. Merkel, J. Phys.: Condens. Matter **18**, S949 (2006).

[30] M. R. Daymond and N. W. Bonner, Mater. Sci. Eng., A **340**, 272 (2003).

Figure captions

FIG. 1 (color online). (a) Axial XRD patterns of the Ge-Au mixture under various pressures. (b) A Rietvelt refinement on the powder x-ray diffraction pattern of the Au-Ge mixture at 11.7 GPa. Both Ge-I and Ge-II phases co-exist and are fitted simultaneously with Au.

FIG. 2 (color online). Deviatoric strain of semiconducting diamond phase Ge (a), metallic β-tin phase Ge (b) and fcc-Au (c) versus pressure.

F IG. 3 (color online). (a) A schematic illustration of the set-up of x-ray diffraction experiments. (b) The ratio of the interplanar spacing of different lattice plane for Au versus pressure. The uncertainty is smaller than the symbol size. (c) Inverse pole figures of gold at 11.9 GPa. (ND: normal direction; RD: rolling direction; TD: transverse direction.)

FIG. 4 SEM images of the sample quenched from 10.65 GPa. The white parts are gold grains and the others are germanium grains.

Figure 1

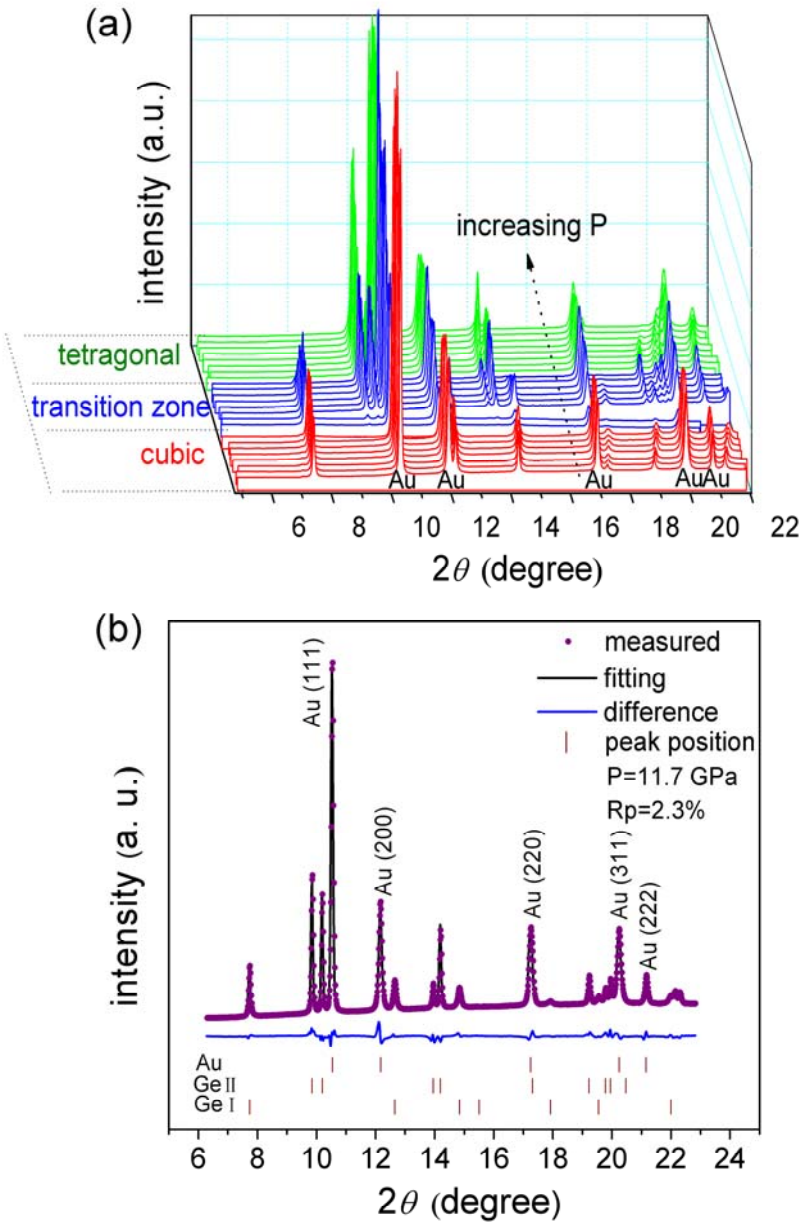
(a)
intensity (a.u.)
increasing P
tetragonal
transition zone
cubic
Au
Au
Au
AuAu
6
8
10
12
14
16
18
20
22
2θ (degree)
(b)
intensity (a. u.)
measured
fitting
difference
peak position
P=11.7 GPa
Rp=2.3%
Au (111)
Au (200)
Au (220)
Au (311)
Au (222)
Au
Ge II
Ge I
6
8
10
12
14
16
18
20
22
24
2θ (degree)

Figure 2

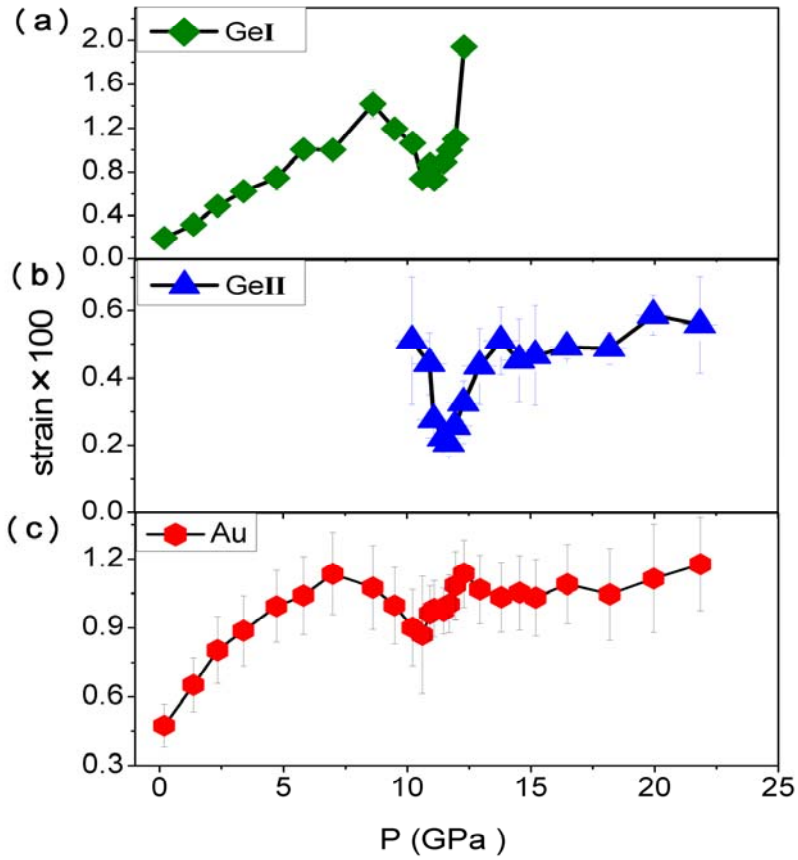
(a)
GeI
2.0
1.6
1.2
0.8
0.4
0.0
(b)
GeII
0.6
0.4
0.2
0.0
strain × 100
(c)
Au
1.2
0.9
0.6
0.3
0
5
10
15
20
25
P (GPa)

Figure 3

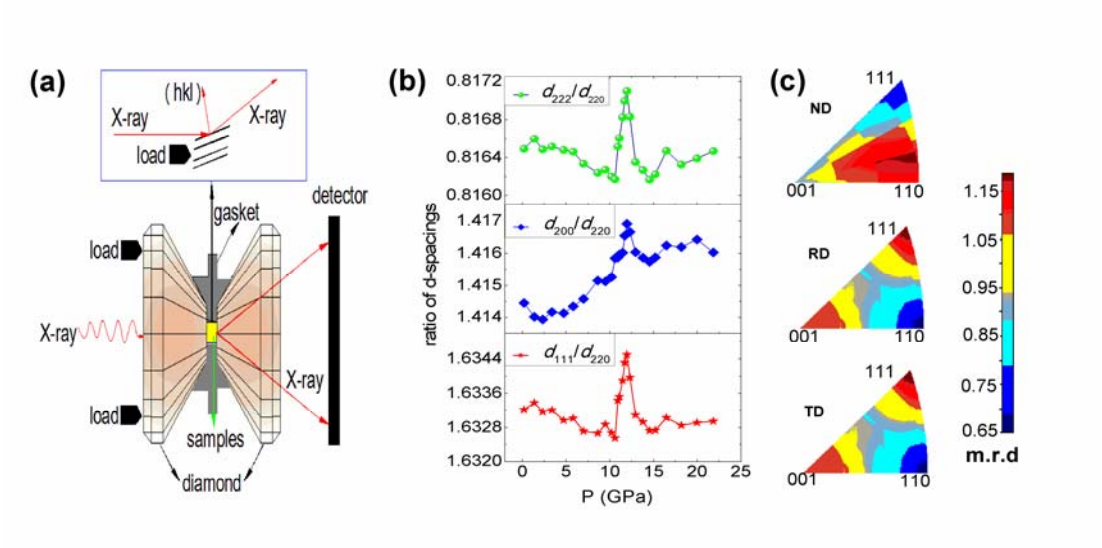
(a)
(hkl)
X-ray
X-ray
load
gasket
detector
load
X-ray
X-ray
load
samples
diamond
(b)
0.8172
0.8168
0.8164
0.8160
d_{222}/d_{220}
1.417
1.416
1.415
1.414
d_{200}/d_{220}
1.6344
1.6336
1.6328
1.6320
d_{111}/d_{220}
ratio of d-spacings
0
5
10
15
20
25
P (GPa)
(c)
111
ND
001
110
111
RD
001
110
111
TD
001
110
1.15
1.05
0.95
0.85
0.75
0.65
m.r.d

Figure 4